Electronic Supplementary Material (ESI) for Journal of Materials Chemistry A.

Supporting information

Plasmon-induced Catalytic CO_2 Hydrogenation by a Nano-sheet Pt/H_xMoO_{3-y} Hybrid with Abundant Surface Oxygen Vacancies

Hao Ge,[a] Yasutaka Kuwahara,*[a,b,c,d] Kazuki Kusu,[a] Hiromi Yamashita*[a,b,c]

[a] Division of Materials and Manufacturing Science, Graduate School of Engineering, Osaka University, 2-1 Yamada-oka, Osaka 565-0871, Japan

[b] Institute for Open and Transdisciplinary Research Initiatives (OTRI), Osaka University, 2-1 Yamada-oka, Suita, Osaka 565-0871, Japan

[c] Unit of Elements Strategy Initiative for Catalysts & Batteries (ESICB), Kyoto University, Katsura, Kyoto 615-8520, Japan

[d] JST, PRESTO, 4-1-8 Hon-Cho, Kawaguchi, Saitama 332-0012, Japan

Content

Table S4. The amount of oxygen vacancy on the surface in Pt/H_xMoO_{3-y} (Bulk, Belt, Rod, Sheet) after H_2 reduction.

Table S5. Summary of the results of XPS measurement for the Pt/H_xMoO_{3-y}(Sheet), Pt/H_xMoO_{3-y}(Sheet)→CO_2 and Pt/H_xMoO_{3-y}(Sheet)→CO_2→H_2.

Figure S14. XPS spectra of Pt/H_xMoO_{3-y}(Sheet)→CO_2+H_2 and Pt/H_xMoO_{3-y}(Sheet)→CO_2: (a) Mo 3*d* XPS spectra, (b) O 1*s* XPS spectra.

Table S6. Summary of the results of XPS measurement for the Pt/H_xMoO_{3-y}(Sheet), Pt/H_xMoO_{3-y}(Sheet)→CO_2 and Pt/H_xMoO_{3-y}(Sheet)→CO_2+H_2.

Figure S15. UV-vis-NIR diffuse reflectance spectra of MoO_3 with different morphologies.

Figure S16. (a) CV test of Pt/H_xMoO_{3-y}(Sheet) with two circles and (b) Photocurrent density of Pt/H_xMoO_{3-y}(Sheet) and Pt/H_xMoO_{3-y}(Sheet)-After CV.

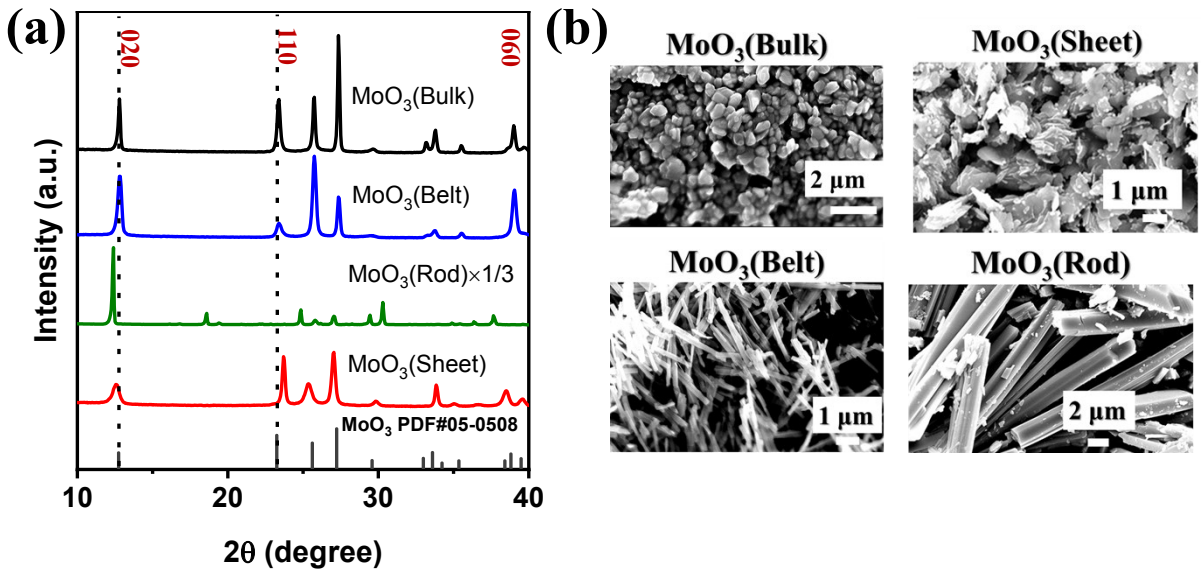

Figure S1. (a) XRD patterns and (b) FE-SEM images of MoO_3 with different morphologies (Bulk, Belt, Rod, Sheet).

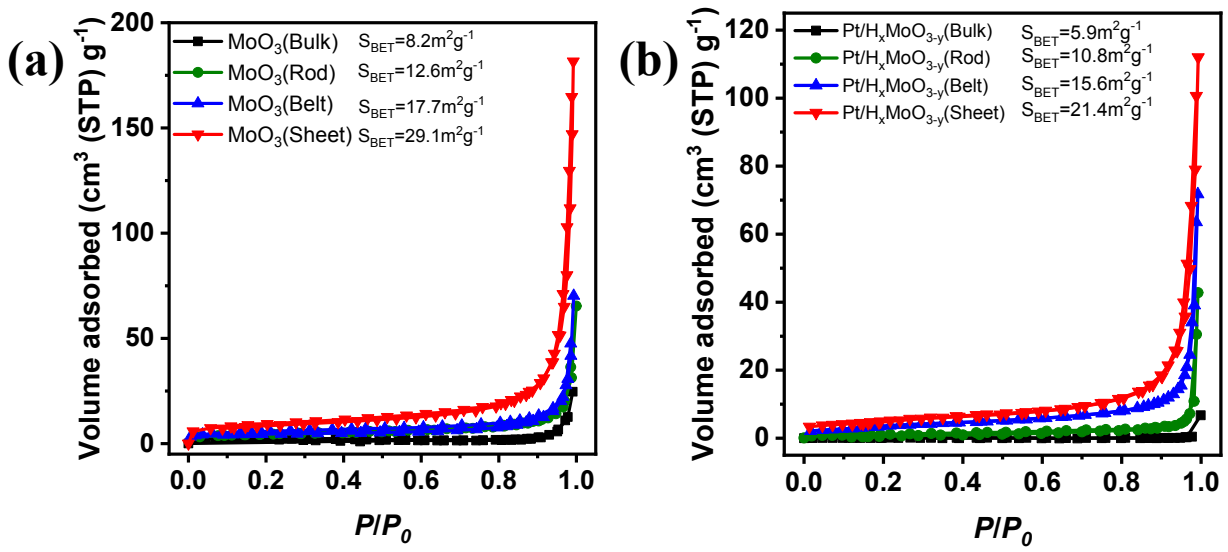

Figure S2. N_2 adsorption-desorption isotherms of (a) MoO_3 (Bulk, Belt, Rod, Sheet) and (b) Pt/H_xMoO_{3-y} (Bulk, Belt, Rod, Sheet).

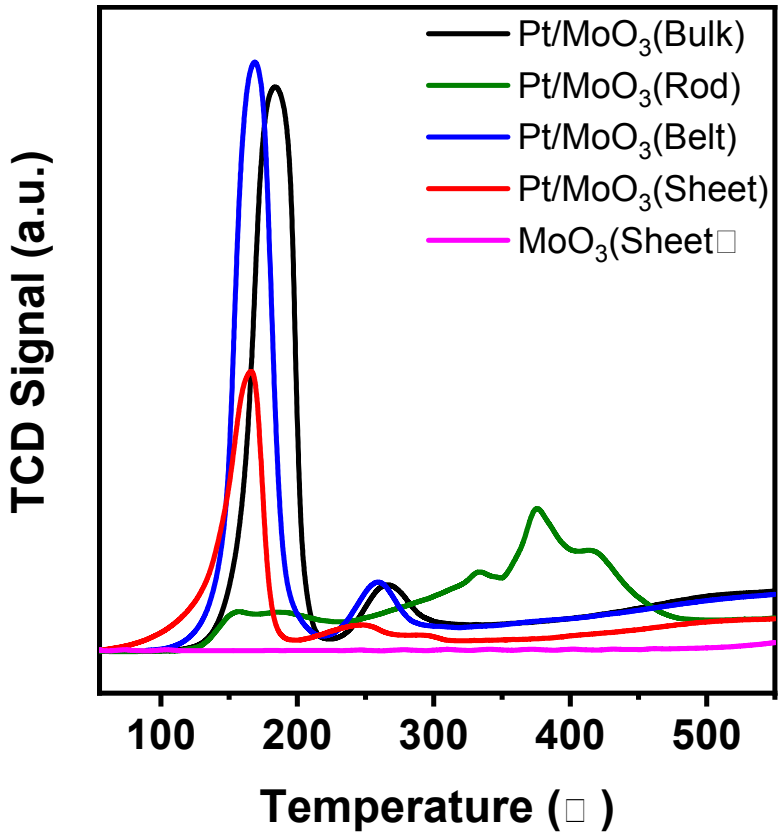

Figure S3. H_2 Temperature programmed reduction (H_2-TPR) profiles of Pt/MoO_3 (Bulk, Belt, Rod, Sheet) and pure MoO_3 (Sheet).

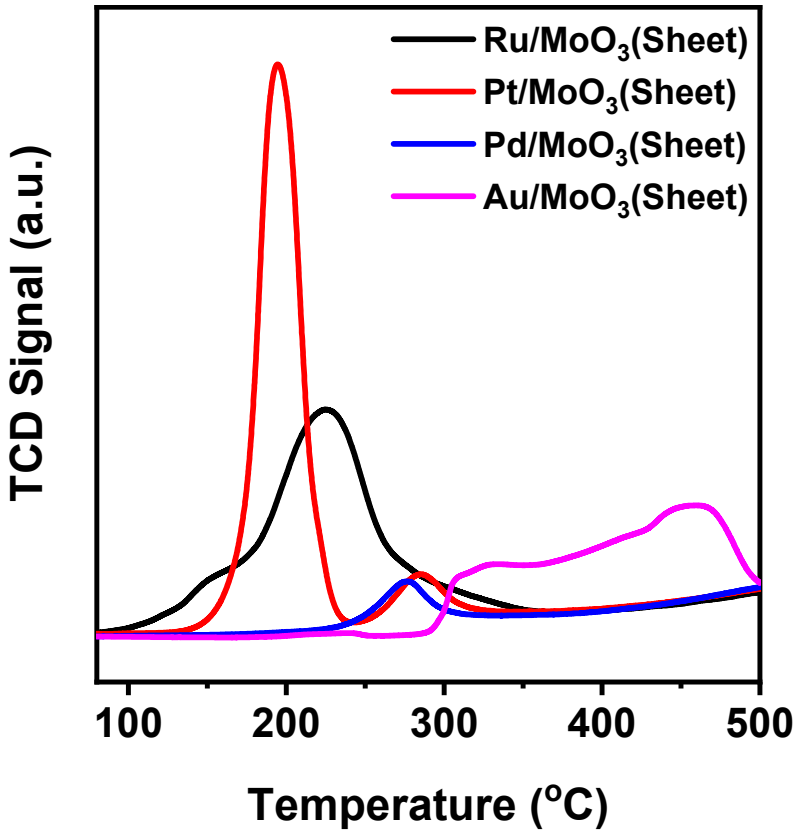

Figure S4. H_2 Temperature programmed reduction (H_2-TPR) profiles of Ru/MoO_3 (Sheet), Pt/MoO_3 (Sheet), Pd/MoO_3 (Sheet) and Au/MoO_3 (Sheet).

Table S1. Performance comparison of different photocatalysts for CO_2 hydrogenation

Catalyst	Gas (CO_2+H_2)	Light Source	T (^oC)	Activity	Ref
Pd@WO_3	1:1	300W Xe lamp	250	3 mmol g^{-1} h^{-1}	1
Rh/Al_2O_3	1:1	300W Xe lamp	360	96.5%	2
$In_2O_{3-x}(OH)_y$	1:1	1000W metal halide bulb	150	1.2 μmol $g^{-1}h^{-1}$	3
Pt/$NaTaO_3$	1:1	300W UV-enhanced Xe lamp	-	139.1 μmol $g^{-1}h^{-1}$	4
Pd@Nb_2O_5	1:1	300W Xe lamp	-	1.8 mmol g^{-1} h^{-1}	5
In_2O_{3-x} nanosheet	1:1	300W Xe lamp	340	103.21 mmol g^{-1} h^{-1}	6
C-In_2O_3	1:1	300W Xe lamp	340	123.41 mmol g^{-1} h^{-1}	7
ncSi:H	1:1	300W Xe lamp	150	250 μmol $g^{-1}h^{-1}$	8
Fe@C hybrid	1:1	300W Xe lamp	-	26.1 mmol g^{-1} h^{-1}	9
Pt/H_xMoO_{3-y}(Sheet)	1:1	500W Hg-Xe short arc lamp	140	1.2 mmol g^{-1} h^{-1}	This work

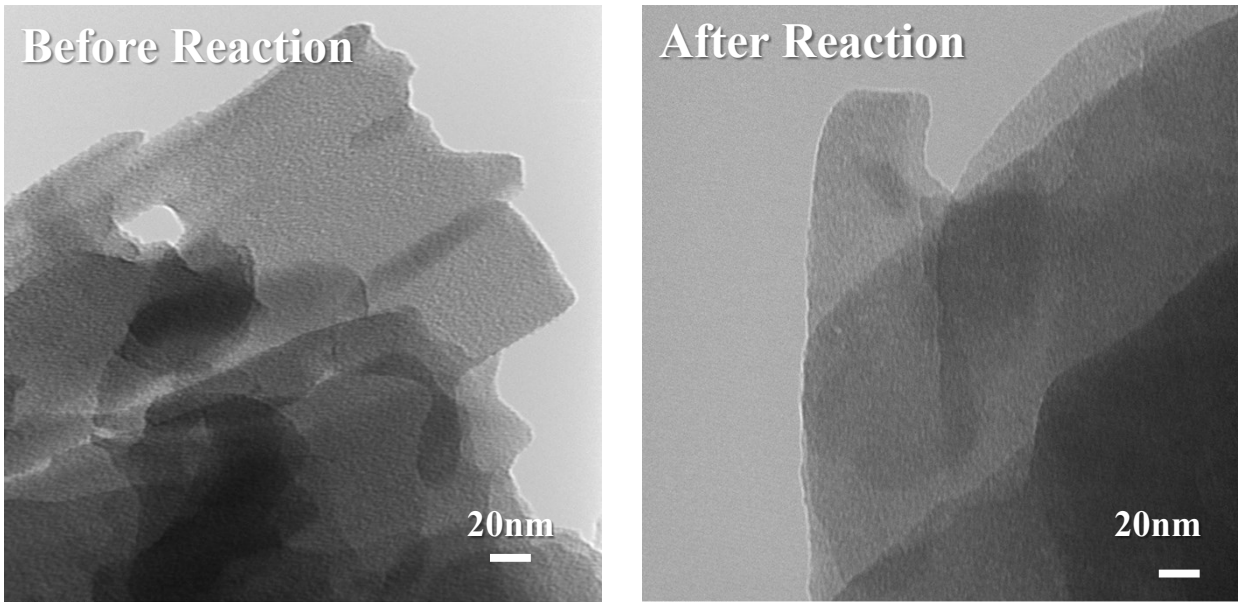

Figure S5. TEM images of Pt/H_xMoO_{3-y}(Sheet) before and after reaction.

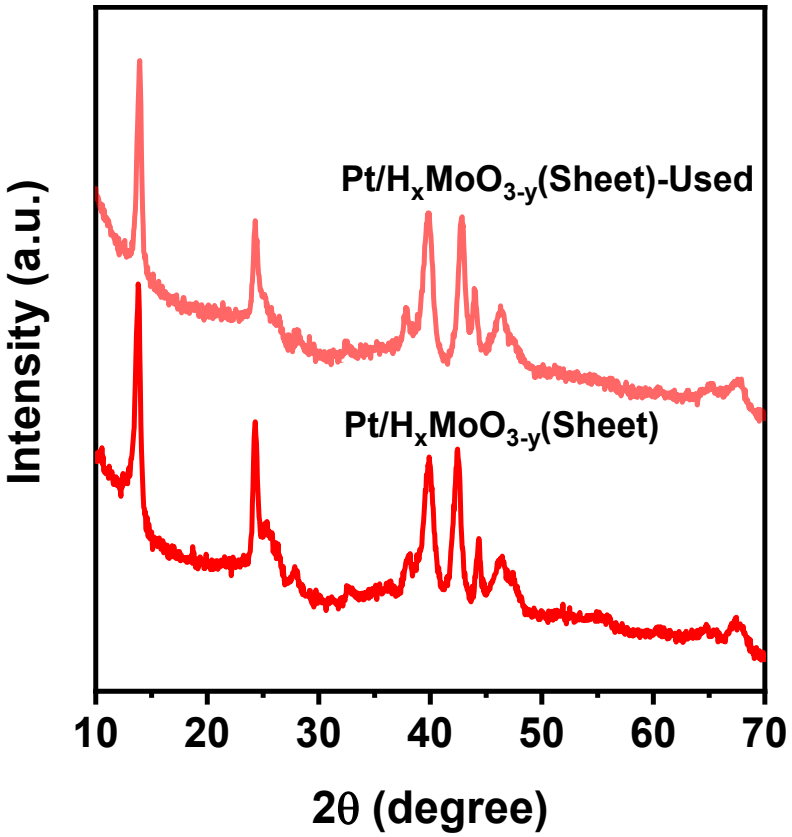

Figure S6. XRD patterns of Pt/$H_x$$MoO_{3-y}$(Sheet) before and after reaction.

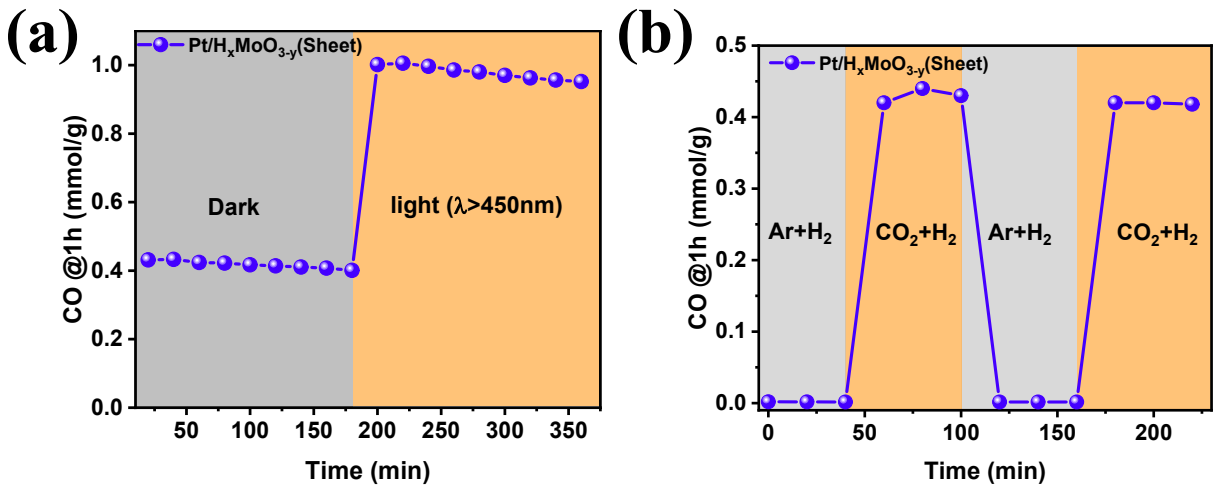

Figure S7. (a) The stability test and (b) gas-switching test of Pt/H_xMoO_{3-y}(Sheet) for photothermal catalytic CO_2 reduction in a flowing system using a fixed-bed reactor system. (Reaction conditions: catalyst (0.1 g), H_2/CO_2 (10/10 mL/min), Xe lamp (λ > 450 nm), Temp. = 140 °C)

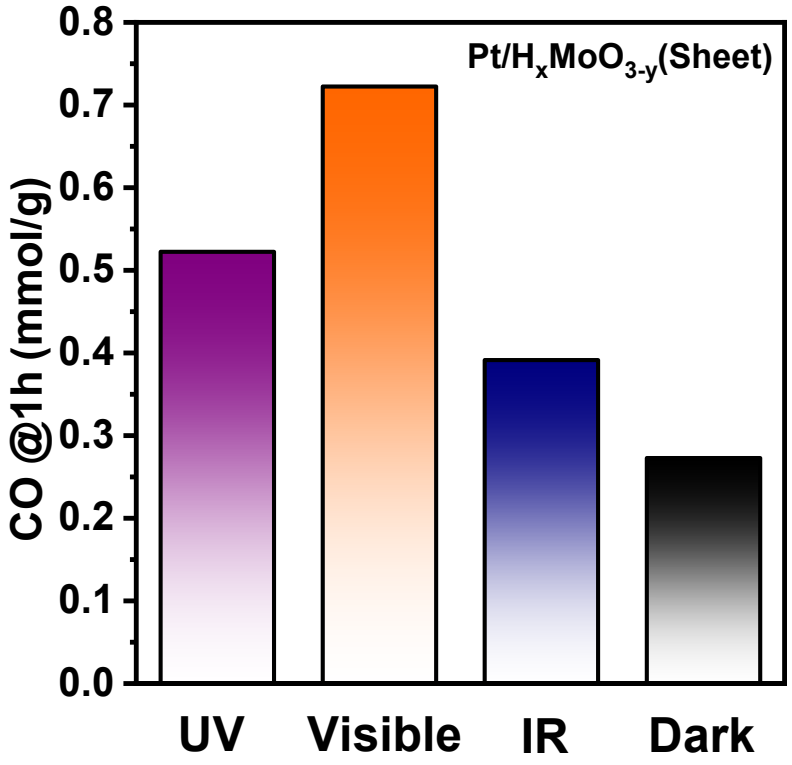

Figure S8. The activity performance of Pt/H_xMoO_{3-y}(Sheet) for photothermal catalytic CO_2 reduction under different light irradiation.

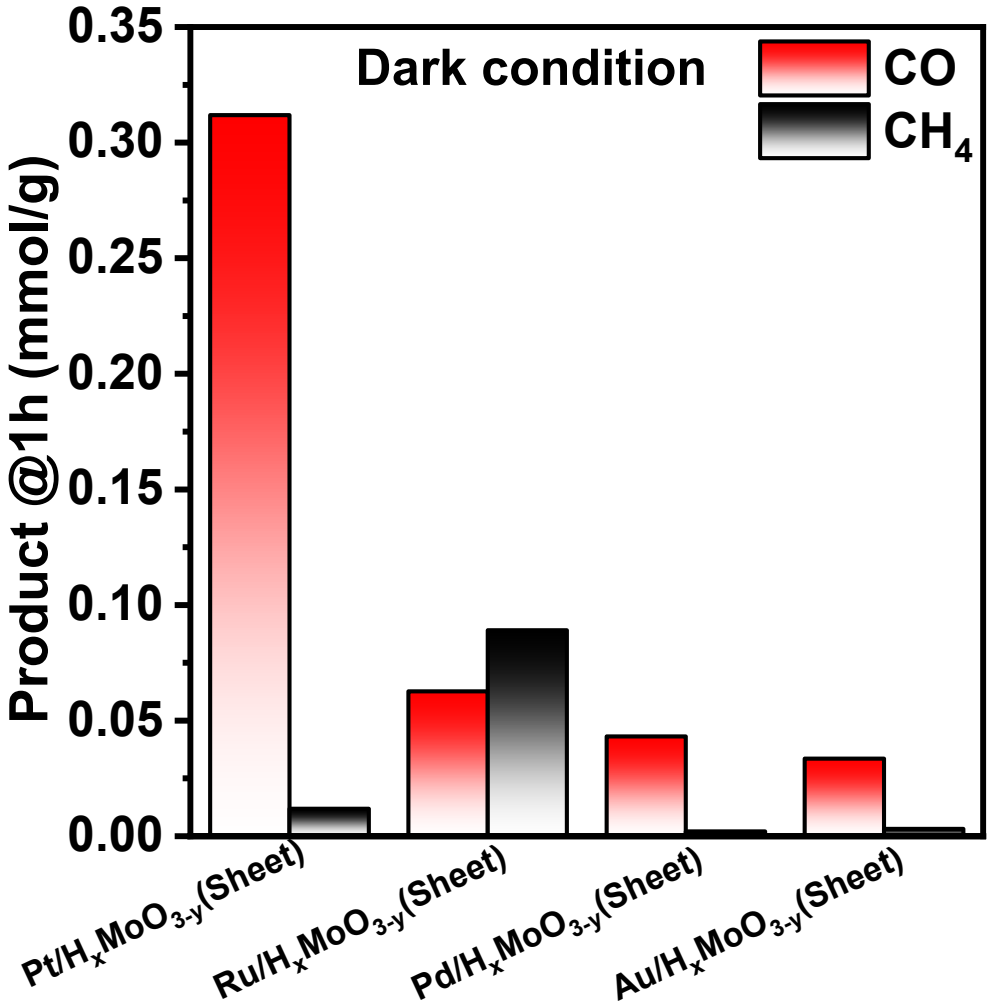

Figure S9. Effect of metal on the catalytic efficiency: Pt/H_xMoO_{3-y}(Sheet), Ru/H_xMoO_{3-y}(Sheet), Pd/H_xMoO_{3-y}(Sheet), and Au/H_xMoO_{3-y}(Sheet). (All of the catalysts were reduced by H_2 at 200 ℃; Reaction conditions: catalyst (0.1 g), H_2: CO_2 (0.5 atm:0.5 atm), light source: $\lambda > 450$ nm, Reaction Temperature: 140 ℃))

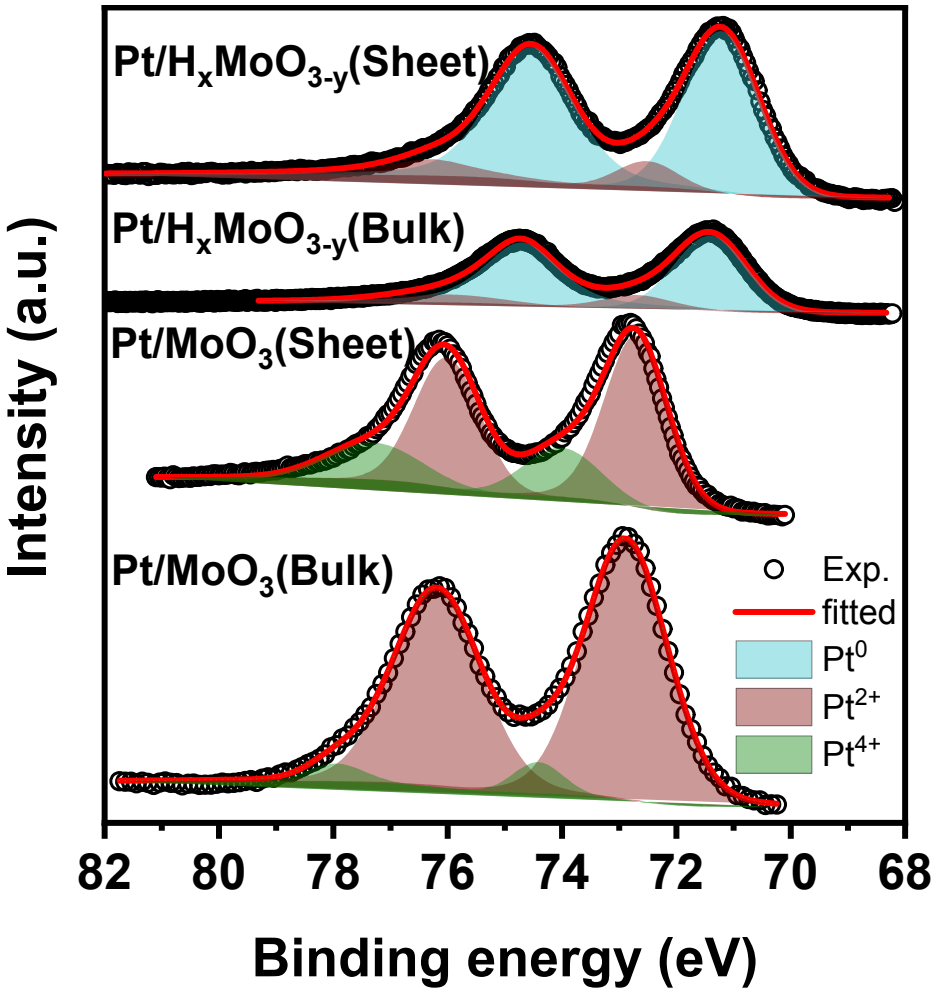

Figure S10. Pt 4*f* XPS spectra of Pt/H_xMoO_{3-y}(Sheet), Pt/H_xMoO_{3-y}(Bulk), Pt/MoO_3(Sheet) and Pt/MoO_3(Bulk).

Table S2. Summary of the results of XPS measurement for the Pt/MoO_3(Bulk), Pt/MoO_3(Sheet), Pt/H_xMoO_{3-y}(Bulk) and Pt/H_xMoO_{3-y}(Sheet).

Sample	Mo 3d XPS				O 1s XPS			
	Mo^{4+} (at%)	Mo^{5+} (at%)	Mo^{6+} (at%)	$(Mo^{4+} + Mo^{5+})/Mo_{total}$	O_L (at%)	O_{-OH} (at%)	O_{H2O} (at%)	$(O_{-OH} + O_{H2O})/O_{total}$
Pt/MoO_3(Bulk)	0	11	89	11	66.1	33.9	0	33.9
Pt/MoO_3(Sheet)	0	81	19	81	58	42	0	42
Pt/H_xMoO_{3-y}(Bulk)	4.9	44.1	51	49	48.5	43.1	9.4	52.5
Pt/H_xMoO_{3-y}(Sheet)	44.4	41.5	14.1	85.9	45	48.5	6.5	55

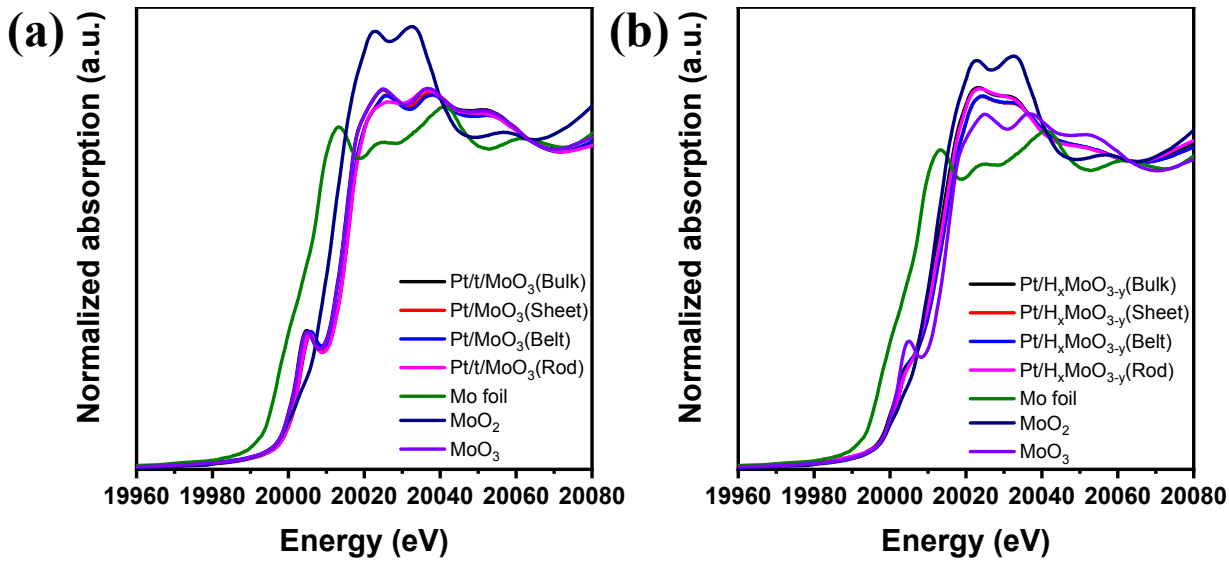

Figure S11. In-situ Mo K-edge X-ray absorption near-edge structure (XANES) spectra of (a) Pt/MoO_3 with different morphologies before reduction and (b) after reduction.

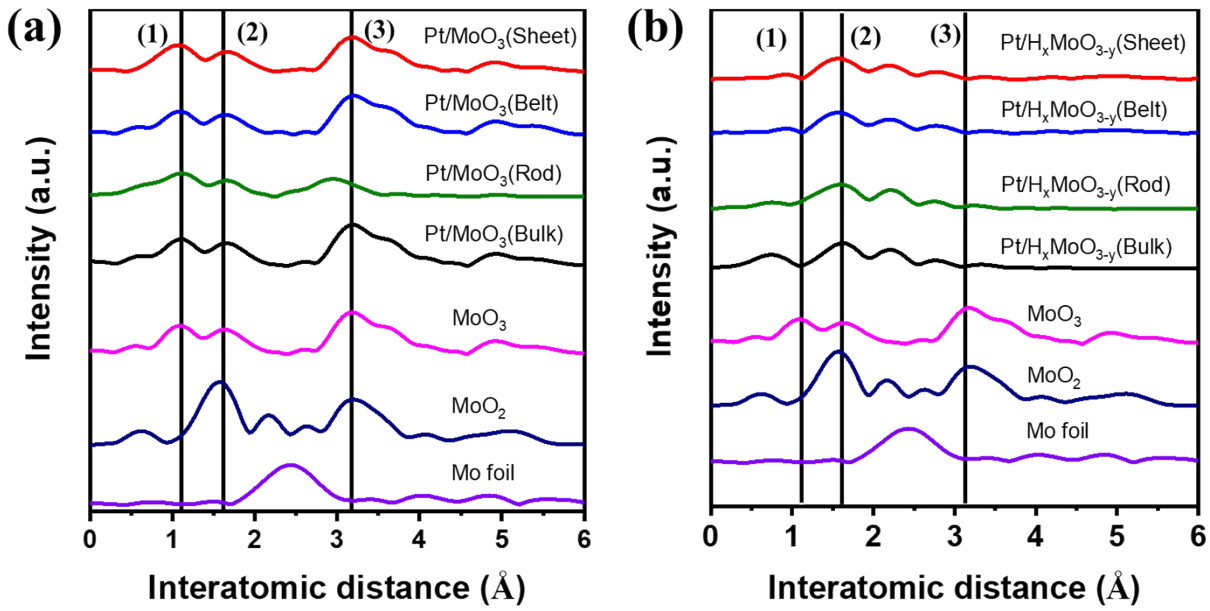

Figure S12. Radial distribution functions (RDFs) of (a) Pt/MoO_3 with different morphologies before reduction and (b) after reduction.

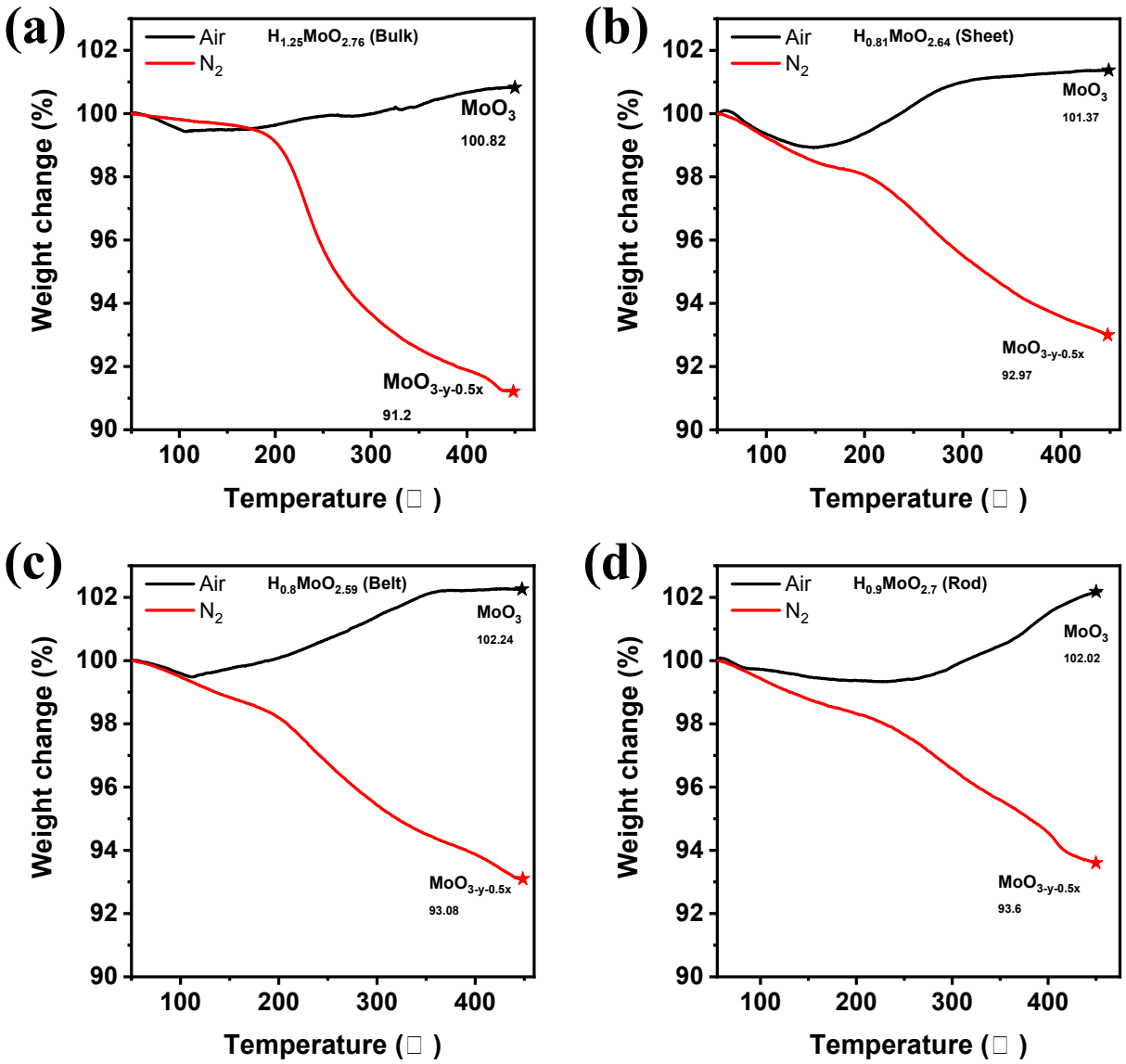

Figure S13. Weight changes of the Pt/H_xMoO_{3-y} with different morphologies (a) Bulk, (b) Sheet, (c) Belt and (d) Rod in a flow of either air or N_2 measured by TG analysis.

In order to quantify the amounts of intercalated H^+ and oxygen vacancies formed in the MoO_3 upon H_2 reduction, thermogravimetric (TG) analysis was carried out in either N_2 or air gas environment. For the Pt/H_xMoO_{3-y} (Bulk, Sheet, Belt, Rod) measured in a N_2 environment, initial weight losses of ~1.0wt% are seen at temperatures below ~100 and 200 °C, respectively, which are due to the evaporation of surface adsorbed water molecules. Subsequently, they show further

weight losses from 200 °C to 450 °C, which are associated with the thermal dehydration of –OH groups to form MoO_{3-x} suboxides ($Pt/H_xMoO_{3-y} \rightarrow MoO_{3-y-x/2} + 1/2x\ H_2O$). By comparing the losing weight differences of each sample at 450 °C, the stoichiometry of intercalated H^+ (x) is calculated to be 1.25, 0.81, 0.8 and 0.9 for Pt/H_xMoO_{3-y}(Bulk), Pt/H_xMoO_{3-y}(Sheet) and Pt/H_xMoO_{3-y}(Belt) and Pt/H_xMoO_{3-y}(Rod), respectively. In comparison, different TG profiles are observed in a flow of air due to the weight gain associated with the filling of oxygen vacancies with molecular O_2 to form MoO_3, in addition to the release of intercalated H^+ as water ($Pt/H_xMoO_{3-y} + O_2 \rightarrow MoO_3 + 1/2x\ H_2O$). For the Pt/H_xMoO_{3-y} (Bulk, Sheet, Belt, Rod) measured in an air environment, a considerable weight gain is seen at temperatures from 200 to 450 °C due to the presence of substantial amount of oxygen vacancy in the sample. By comparing the weight gain differences of each sample at 450 °C, the stoichiometry of oxygen vacancy (y) is calculated to be 0.24, 0.34, 0.4 and 0.29 for Pt/H_xMoO_{3-y}(Bulk), Pt/H_xMoO_{3-y}(Sheet), Pt/H_xMoO_{3-y}(Belt) and Pt/H_xMoO_{3-y}(Rod), respectively.

Table S3. The concentration of intercalated H^+ and oxygen vacancy in the samples.

Sample	Concentration of intercalated H^+ (x)	concentration of oxygen vacancies (y)
Pt/H_xMoO_{3-y}(Bulk)	1.25	0.24
Pt/H_xMoO_{3-y}(Sheet)	0.81	0.34
Pt/H_xMoO_{3-y}(Belt)	0.8	0.4
Pt/H_xMoO_{3-y}(Rod)	0.9	0.29

Table S4. The amount of oxygen vacancy on the surface in Pt/H_xMoO_{3-y} (Bulk, Belt, Rod, Sheet) after H_2 reduction.

Sample	The amount of surface oxygen vacancy (μmol·g-cat^{-1})
Pt/H_xMoO_{3-y}(Bulk)	446
Pt/H_xMoO_{3-y}(Sheet)	664
Pt/H_xMoO_{3-y}(Belt)	332
Pt/H_xMoO_{3-y}(Rod)	270

Determination of surface oxygen vacancy

The oxygen vacancy on the surface of the catalyst can capture the oxygen of the diphenyl sulfoxide to produce diphenyl sulfide. The oxygen vacancy in MoO_3 cannot be regenerated in dark without H_2 gas. The reaction will stop when the surface oxygen vacancy of MoO_3 is exhausted. Therefore, this reaction can be used to calculate the number of surface oxygen vacancies with different morphologies of MoO_3 by counting the yield of diphenyl sulfide. The reaction operation as follows: First, add 50 mg catalyst to the quartz tube and seal the nozzle for H_2 reduction with the temperature of 200 ℃, and the hydrogen reduction process was maintained for 30 minutes. After that, argon gas is introduced into the quartz tube for 20 minutes to expel the hydrogen. And add the reaction solution into the quartz tube (Diphenyl sulfoxide:0.2mmol; Diphenyl: 0.1mmol; Methylbenzene: 10mL). Finally, 0.1mL of the reaction solution is taken out and analyzed by GC.

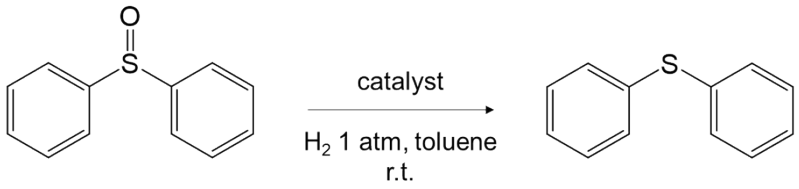

Scheme S1. Deoxygenation of diphenyl sulfoxide to phenyl sulfide using molecular H_2 as a reductant.

Table S5. Summary of the results of XPS measurement for the Pt/H_xMoO_{3-y}(Sheet), Pt/H_xMoO_{3-y}(Sheet)→CO_2 and Pt/H_xMoO_{3-y}(Sheet)→CO_2→H_2.

Sample	Mo 3*d* XPS				O 1*s* XPS			
	Mo^{4+} (at%)	Mo^{5+} (at%)	Mo^{6+} (at%)	$(Mo^{4+} + Mo^{5+})/Mo_{total}$	O_L (at%)	O_{-OH} (at%)	O_{H2O} (at%)	$(O_{-OH} + O_{H2O})/O_{total}$
Pt/H_xMoO_{3-y} (sheet)	44.4	41.5	14.1	85.9	45	48.5	6.5	55
Pt/H_xMoO_{3-y} (sheet)→CO_2	22.3	24.3	53.4	46.6	58.5	33.7	7.8	41.5
Pt/H_xMoO_{3-y} (Sheet)→CO_2→H_2	63.3	23.7	13	87	43.6	48.2	8.2	56.4

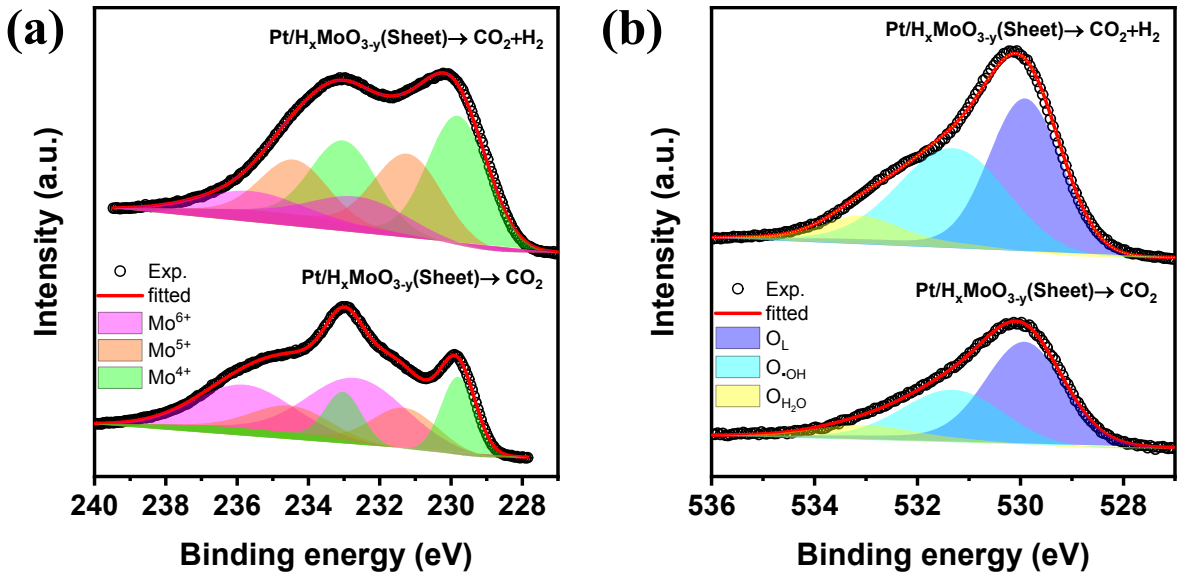

Figure S14. XPS spectra of Pt/H_xMoO_{3-y}(Sheet)→CO_2+H_2 and Pt/H_xMoO_{3-y}(Sheet)→CO_2: (a) Mo 3*d* XPS spectra, (b) O 1*s* XPS spectra.

Table S6. Summary of the results of XPS measurement for the Pt/H_xMoO_{3-y}(Sheet), Pt/H_xMoO_{3-y}(Sheet)→CO_2 and Pt/H_xMoO_{3-y}(Sheet)→CO_2+H_2

Sample	Mo 3*d* XPS				O 1*s* XPS			
	Mo^{4+} (at%)	Mo^{5+} (at%)	Mo^{6+} (at%)	$(Mo^{4+}+Mo^{5+})/Mo_{total}$	O_L (at%)	O_{-OH} (at%)	O_{H2O} (at%)	$(O_{-OH}+O_{H2O})/O_{total}$
Pt/H_xMoO_{3-y} (sheet)	44.4	41.5	14.1	85.9	45	48.5	6.5	55
Pt/H_xMoO_{3-y} (sheet)→CO_2	22.3	24.3	53.4	46.6	58.5	33.7	7.8	41.5
Pt/H_xMoO_{3-y} (Sheet)→CO_2+H_2	50.3	32.9	16.8	83.2	47.6	44	8.4	52.4

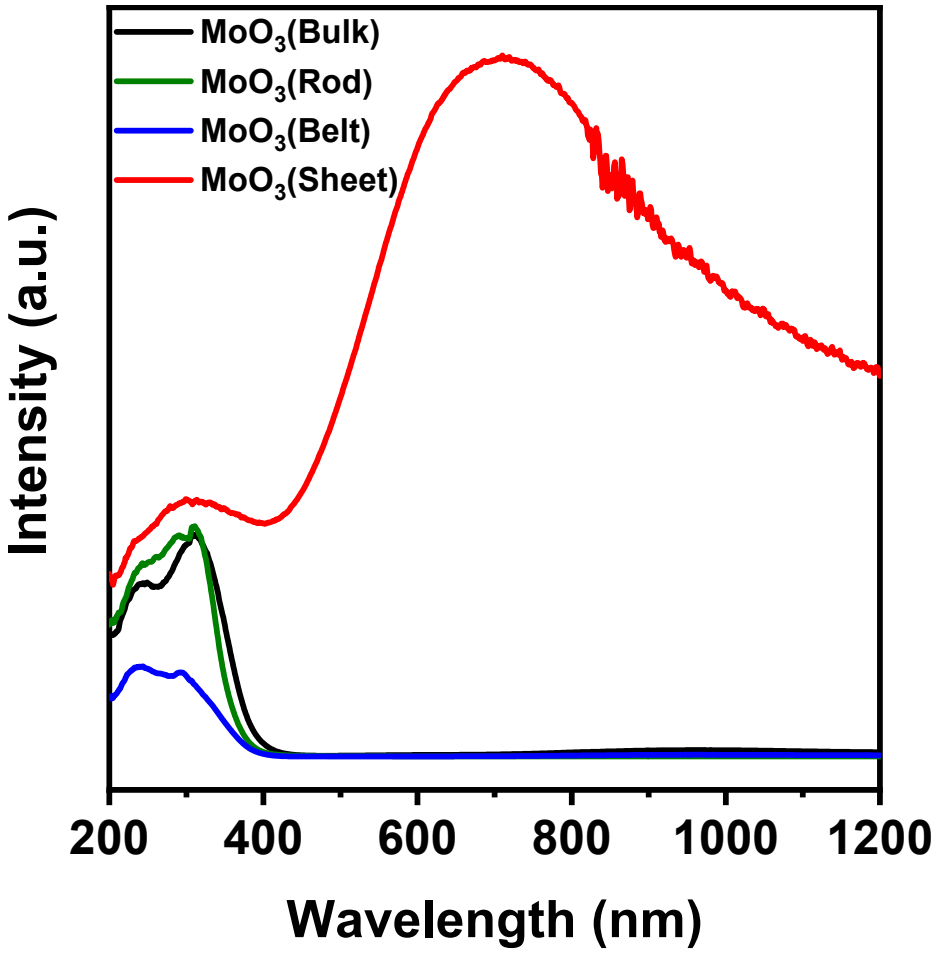

Figure S15. Diffuse reflectance UV-vis-NIR spectra of MoO_3 with different morphologies.

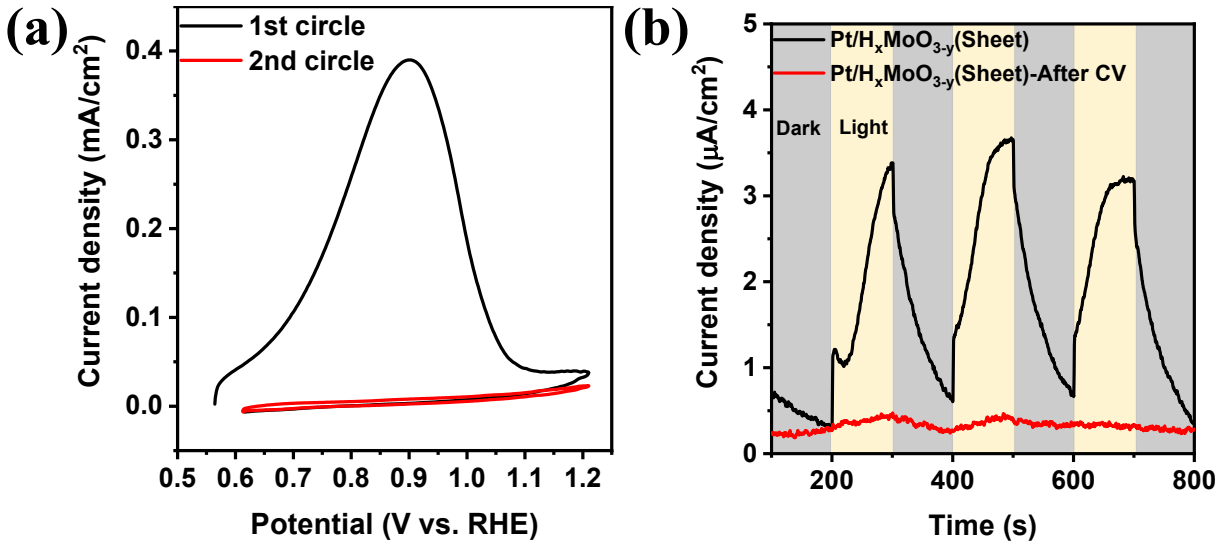

Figure S16. (a) CV test of Pt/H_xMoO_{3-y}(Sheet) with two circles and (b) Photocurrent density of Pt/H_xMoO_{3-y}(Sheet) and Pt/H_xMoO_{3-y}(Sheet)-After CV.

References

1 Y. F. Li, N. Soheilnia, M. Greiner, U. Ulmer, T. Wood, A. A. Jelle, Y. Dong, A. P. Yin Wong, J. Jia and G. A. Ozin, ACS Appl. Mater. Interfaces, 2019, 11, 5610–5615.

2 X. G. Meng, T. Wang, L. Q. Liu, S. X. Ouyang, P. Li, H. L. Hu, T. Kako, H. Iwai, A. Tanaka, J. H. Ye, Angew. Chem. Int. Ed. 2014, 53, 11478.

3 L. He, T. E. Wood, B. Wu, Y. C. Dong, L. B. Hoch, L. M. Reyes, D. Wang, C. Kubel, C. X. Qian, J. Jia, K. Liao, P. G. O'Brien, A. Sandhel, J. Y. Y. Loh, P. Szymanski, N. P. Kherani, T. C. Sum, C. A. Mims, G. A. Ozin, ACS Nano. 2016, 10, 5578.

4 J. Jia, P. G. O'Brien, L. He, Q. Qiao, T. Fei, L. M. Reyes, T. E. Burrow, Y. C. Dong, K. Liao, M. Varela, S. J. Pennycook, M. Hmadeh, A. S. Helmy, N. P. Kherani, D. D. Perovic, G. A. Ozin, Adv. Sci. 2016, 3, 1600189.

5 H. B. Zhang, T. Wang, J. J. Wang, H. M. Liu, T. D. Dao, M. Li, G. G. Liu, X. G. Meng, K. Chang, L. Shi, T. Nagao, J. H. Ye, Adv. Mater. 2016, 28, 3703.

6 Y. Qi, L. Song, S. Ouyang, X. Liang, S. Ning, Q. Zhang, J. Ye, Adv. Mater. 2019, 32, 1903951.

7 Y. Qi, J. Jiang, X. Liang, S. Ouyang, W. Mi, S. Ning, L. Zhao, and J. Ye, Adv. Funct. Mater. 2021, 2100908.

8 M. Li, P. Li, K. Chang, T. Wang, L. Q. Liu, Q. Kang, S. X. Ouyang, J. H. Ye, Chem. Commun. 2015, 51, 7645.

9 J. Ren, S. X. Ouyang, H. Xu, X. G. Meng, T. Wang, D. F. Wang, J. H. Ye, Adv. Energy Mater. 2017, 7, 1601657.